NeuroImage 208 (2020) 116466

Contents lists available at ScienceDirect

NeuroImage

journal homepage: www.elsevier.com/locate/neuroimage

Validating faster DENSE measurements of cardiac-induced brain tissue expansion as a potential tool for investigating cerebral microvascular pulsations

Ayodeji L. Adams [a,*], Max A. Viergever [b], Peter R. Luijten [a], Jaco J.M. Zwanenburg [a]

[a] Department of Radiology, University Medical Center Utrecht, E 01.132, Heidelberglaan 100, 3584 CX, Utrecht, the Netherlands
[b] Image Sciences Institute, University Medical Center Utrecht, Heidelberglaan 100, 3584 CX, Utrecht, the Netherlands

ARTICLE INFO

Keywords:
Brain
Displacement
Microvasculature
Pulsatility
Intracranial dynamics
CSF

ABSTRACT

Displacement Encoding with Stimulated Echoes (DENSE) has recently shown potential for measuring cardiac-induced cerebral volumetric strain in the human brain. As such, it may provide a powerful tool for investigating the cerebral small vessels. However, further development and validation are necessary. This study aims, first, to validate a retrospectively-gated implementation of the DENSE method for assessing brain tissue pulsations as a physiological marker, and second, to use the acquired measurements to explore intracranial volume dynamics. We acquired repeated measurements of cerebral volumetric strain in 8 healthy subjects, and internally validated these measurements by comparing them to spinal CSF stroke volumes obtained in the same scan session.

Peak volumetric strain was found to be highly repeatable between scan sessions. First/second measured peak volumetric strains were: $(6.4 \pm 1.7)x10^{-4}/(6.7 \pm 1.6)x10^{-4}$ for whole brain, $(9.5 \pm 2.5)x10^{-4}/(9.6 \pm 2.4)x10^{-4}$ for grey matter, and $(4.4 \pm 1.7)x10^{-4}/(4.1 \pm 0.8)x10^{-4}$ for white matter. Grey matter showed significantly higher peak strain ($p < 0.001$) and earlier time-to-peak strain ($p < 0.02$) than white matter. An approximately linear relationship was found between CSF and brain tissue volume pulsations over the cardiac cycle (mean slope and R^2 of 0.88 ± 0.23 and 0.89 ± 0.07, respectively). The close similarity between CSF and brain tissue volume pulsations implies limited contributions from large intracranial vessel pulsations, providing further evidence for venous compression as an additional mechanism for maintaining stable intracranial pressures over the cardiac cycle.

Cerebral pulsatility showed consistent inter-subject peak values in healthy subjects, and was strongly correlated to CSF stroke volumes. These results strengthen the potential of brain tissue volumetric strain as a means for investigating the intracranial dynamics of the ageing brain in normal or diseased states.

1. Introduction

The small vessels which compose the cerebral microvasculature pulsate as a result of transient increases in intracranial blood volume during the cardiac cycle, thereby causing local tissue displacement (Sweetman and Linninger, 2011). Recently, we used an MR imaging technique called Displacement Encoding with Stimulated Echoes (DENSE) (Aletras et al., 1999) to measure the pulsatile brain tissue motion and indirectly investigate changes in the microvascular blood volume over the cardiac cycle (Adams et al., 2019). From the brain tissue motion, volumetric strain (change in tissue volume ΔV relative to the original volume V:$\varepsilon_v = \frac{\Delta V}{V}$) was computed. Peak volumetric strain showed differences between grey matter and white matter that matched the relative blood volume differences between these two tissue types, suggesting that tissue volumetric strain reflects swelling of the microvasculature embedded in the tissue. The ability to study the swelling of the microvasculature bed within the brain would be an advantage of DENSE over 'mass-balance' approaches that study blood- and CSF flows at the spinal canal (Balédent

Abbreviations: AP, Anterior-Posterior; cSVD, Cerebral Small Vessel Disease; DENSE, Displacement Encoding with Stimulated Echoes; FH, Feet-Head; ICVC, Intracranial Volume Change; PCMRI, Phase-contrast Magnetic Resonance Imaging; POx, Pulse Oximeter; RL, Right-Left; ROI, Region of Interest; SNR, Signal-to-Noise Ratio; VCG, Vectorcardiogram.

* Corresponding author. University Medical Center Utrecht, Internal Post Number: E01132, P.O Box: 85500, 3508 GA, Utrecht, the Netherlands.
E-mail addresses: a.l.adams-5@umcutrecht.nl (A.L. Adams), M.Viergever@umcutrecht.nl (M.A. Viergever), P.Luijten@umcutrecht.nl (P.R. Luijten), J.J.M.Zwanenburg@umcutrecht.nl (J.J.M. Zwanenburg).

https://doi.org/10.1016/j.neuroimage.2019.116466
Received 19 November 2019; Accepted 13 December 2019
Available online 13 December 2019

et al., 2001; Wåhlin et al., 2012), which cannot distinguish blood volume changes originating from the large vessels in the subarachnoidal CSF and volume changes originating from the vascular bed in the brain tissue.

Although DENSE comes at the cost of a factor of 2 in signal-to-noise (compared to a spin echo), it is an ideal method for investigating sub-voxel brain tissue motion as it permits the spatial quantification of sub-millimeter tissue motion, and inherently limits eddy current induced phase errors by temporally separating the motion encoding/decoding gradients through the use of a stimulated echo acquisition. For comparison, an optimized phase contrast velocity method would need an encoding velocity (V_{enc}) of about 1 mm/s (approx. maximally 300 μm motion during systole (Adams et al., 2019; Soellinger et al., 2009)), which implies the need for impractically large bipolar gradients, or a large loss in signal-to-noise due to the use of a strongly suboptimal V_{enc}. However, further development and validation of DENSE-derived volumetric strain measurements are necessary to ascertain the feasibility of this approach for investigating the changes to the cerebral microvasculature which may occur naturally with age or with disease. Previous measurements of brain tissue pulsatility were lengthy due to the use of a triggered acquisition that required scanning 120% of the cardiac cycle to obtain full coverage of the cardiac cycle. This effectively led to a repetition time between the motion encodings of two heartbeats (double scan duration), increasing the likelihood of motion artefacts and reducing the clinical viability of the method. Improvements to the acquisition scheme are therefore needed to allow full coverage of the cardiac cycle in a more efficient manner. Additionally, measurement repeatability would offer an insight into whether inter-subject peak volumetric strain variability reflects physiological variation or simply sensitivity of the volumetric strain calculation to noise. Furthermore, internal validation of brain tissue volumetric strain could be achieved through measurements of CSF stroke volume during the same scan session (as the cranial vault has a fixed volume, swelling of brain tissue or the arterial compartments must be compensated by displacing CSF spinally (Enzmann and Pelc, 1993; Greitz et al., 1992)).

This study aims, first, to validate a more efficient DENSE method for assessing brain tissue pulsations as a physiological marker, and second, to use the acquired measurements to explore intracranial volume dynamics. To achieve these aims, we first implemented a retrospectively-gated version of DENSE, which reduced the acquisition duration by half, and assessed the repeatability of the brain tissue volumetric strain by performing repeated measurements on healthy subjects. The cardiac-induced volumetric strain was analysed for the whole brain, as well as for grey and white matter tissue separately. Second, for internal validation we measured the CSF spinal stroke volumes as independent physiological measurements of the subjects. Finally, we used the CSF and DENSE measurements to further explore the physiology of intracranial volume dynamics by disentangling the contributions of the large intracranial extracerebral vessels and the cerebral microvasculature to spinally displaced CSF.

2. Materials and methods

2.1. Measurements

To investigate the repeatability of brain tissue volumetric strain measurements, the DENSE protocol was performed twice within a 2-h period on the same day, with repositioning of the subjects. For the comparison of the DENSE measurements with an independent measurement in the same subjects, a CSF flow scan was also acquired. Informed consent for all measurements was obtained from 8 healthy young subjects of European descent without known cardiovascular or cerebral diseases (3 females, mean age: 27 ± 6) to participate in the study, which was approved by the governing Ethical Review Board of our institution.

In the first scan session, three 4D (3D + time) brain tissue displacement measurements were acquired on a 7T MR scanner (Philips Healthcare) on which we implemented retrospectively-gated DENSE (Adams et al., 2018). Similar to previous work (Adams et al., 2019), the three DENSE acquisitions covered the entire cardiac cycle in the right-left (RL), anterior-posterior (AP) and feet-head (FH) directions, and were acquired using opposite gradient polarities. Retrospectively-gated phase-contrast MRI (PCMRI) was used to acquire time-resolved 2D CSF flow measurements at the C2-C3 level. The PCMRI acquisition was sensitised for motion in the FH direction. Both DENSE and PCMRI measurements were performed using a 32 channel head coil (Nova Medical), and synchronised to the cardiac cycle using a pulse oximeter (POx) attached to the index finger on the left hand.

After the first scan session, subjects were briefly taken out of the MR scanner and allowed to move around freely (for a maximum of 10 min) before being repositioned into the scanner for the second scan session. During the second scan session, subjects were re-scanned using the same DENSE protocol as the first session.

Additionally, a 3D T1-weighted FFE scan was also made for both scan sessions for registration and segmentation of the brain tissue. See Table 1 for all relevant scan parameters.

2.2. Analysis

An identical analysis was performed on the DENSE images acquired from each scan session. The analysis comprised of several steps as described below.

2.2.1. Background phase removal

Background phase errors could be removed by subtraction of the two opposing gradient polarity images present for each DENSE acquisition.

Table 1
Imaging parameters used in the study.

Parameter	T1-weighted FFE	DENSE	PCMRI
Denc[a] (mm) (FH/AP/RL)	–	0.35/0.175/0.175	–
Venc[b] (cm/s) (FH)	–	–	5
Resolution (mm) (FHxAPxRL)	0.93 × 0.93 x 1	1.95 × 1.95 x 2.2	3 × 0.45 x 0.45
FOV (mm) (FHxAPxRL)	300 × 248 × 190	250 × 250 × 190	3 × 190 × 185
TR (ms)	4	35/30/35 (FH/AP/RL)	12
TE (ms)	2	8.7	6.1
EPI factor	–	15	–
TFE factor	600	2	2
Readout/phase BW (Hz/pixel)	405/–	2342/92	474/–
Inversion delay (ms)	1235	–	–
Max. gradient strength (mT/m)	40	30	25
Max. gradient slew rate (T/m/s)	200	150	150
SENSE (APxRL)	2 × 2	1.9 × 2.5	1 × 2
Flip angle (deg)	5	Variable[c]	30
Cardiac synchronisation[d]	–	Retrospective	Retrospective
Phases/cardiac cycle	–	20	36–40
Scan duration (min:s)[e]	0:48	2:24	1:43

[a] Denc: motion (either positive or negative) that induces phase wrap in the subtracted phase images, analogous to the Venc parameter in velocity encoded phase contrast imaging.
[b] Velocity was measured in the FH direction. One subject was scanned with a Venc = 10 cm/s to eliminate phase wraps.
[c] The flip angles were varied over the cardiac cycle to create a stable signal (Stuber et al., 1999), assuming a T1 of 1100 ms. The maximum flip angle in the sweep was set to 30°, in order to maintain/preserve longitudinal magnetization for tagging at the next cardiac cycle.
[d] The retrospectively-gated acquisitions were performed using a pulse oximeter as the triggering device, which was attached to the left index finger.
[e] Scan duration reported for a heart rate of 60 beats/min and for one motion encoding direction.

However, we observed that the background phase was stable for every acquired phase of cardiac cycle. Therefore, we preferred to remove the background phase by subtracting the first acquired cardiac phase from all others, with the minor consequence of introducing an arbitrary offset which was irrelevant for our peak-to-peak based analysis. This has the benefit that the volumetric strain can be computed from the DENSE displacement fields for each gradient polarity separately, and later combined (after inversion of the negative gradient polarity. This allowed us to do artefact removal for each gradient polarity image, rather than on the level of the subtracted images.

2.2.2. Image registration

Registration of the DENSE images was performed to correct for typical EPI distortions and subject motion between each displacement-sensitive acquisition. First, AP and FH magnitude images were rigidly registered to RL magnitude images to correct for subject motion between acquisitions. Next, the last RL magnitude image of the cardiac cycle was non-rigidly registered using Elastix (Klein et al., 2010) to the subject's high resolution T1-weighted image (RL magnitude images were used for the non-rigid registration, as these images showed virtually no artefacts at the end of the cardiac cycle, where image contrast between grey matter and white matter was optimal). Finally, all images were transformed to the T1-weighted image using the non-rigid registration parameters obtained from the registration of the RL image to the T1-weighted image. The magnitude and phase images were combined to form complex images before transformation to the T1-weighted image space to prevent interpolation errors near phase jumps.

2.2.3. Brain tissue selection

A brain tissue mask free of large blood vessels, CSF and artefacts must be used to obtain a volumetric strain map which reflects only changes induced by the swelling of the microvasculature embedded in the tissue. A brain tissue mask without the large blood vessels was created by using the Computational Anatomy Toolbox (Jena University Hospital, Departments of Psychiatry and Neurology) extension for SPM12 (Wellcome Trust Centre for Neuroimaging, University College London). The software yields CSF, grey and white matter probability maps from the T1-weighted image which were used to segment the T1-weighted image into CSF, grey and white matter tissue. The large intracranial blood vessels were associated with high intensities in the T1-weighted image, and were therefore incorrectly marked as grey or white matter by SPM12. These large blood vessels were removed from the grey and white matter probability masks using morphological area opening. Voxels in the grey and white matter tissue masks with a probability less than 0.95, or a CSF probability greater than zero (as determined by SPM12) were subsequently removed.

2.2.4. Artefact removal

Physiological motion that is not synchronised with the triggering device, leads to an inter-shot phase instability and thus image artefacts. The sensitivity to such motion increases with increasing delay between motion-encoding and –decoding, and is, thus, maximal at the end of the cardiac cycle. As subjects have most freedom to move in the FH direction, while breathing causes a roll over the AP-axis (Sloots et al., 2018) (mimicking FH motion in the frontal areas of the brain), these artefacts in the DENSE images are most extreme in the FH acquisitions (Adams et al., 2019; Soellinger et al., 2009)). These artefacts were typically characterised in the magnitude images by a rapidly decaying image intensity throughout the latter half of the cardiac cycle (see Fig. S1 in Supplementary Material). This characteristic was used to be remove the artefacts from the brain tissue masks used for the volumetric strain analysis. The spatial location of the artefacts was different in each gradient polarity image, an observation which we exploited to maximise the brain region available for the analysis. The artefacts were detected and removed from the whole brain tissue mask as follows.

First, an estimate of the DENSE signal-to-noise ratio (SNR) for each gradient polarity was created by dividing the magnitude image from the end of the cardiac cycle (when the artefacts were most prominent) by the temporal standard deviation as defined in Eqn (1),

$$SNR[i,j,k] = \frac{Mag[i,j,k,n]}{\sqrt{\frac{\sum_{t=1}^{n}\left(Mag[i,j,k,t]-\frac{1}{n}\sum_{t=1}^{n}Mag[i,j,k,t]\right)^2}{n-1}}} \quad \text{Eqn 1}$$

where *i,j,k* are image coordinates and $t = 1$ represents the first of n acquired cardiac phases.

Secondly, the estimated SNR map was thresholded to create a mask free of artefacts. A threshold value of five was empirically determined to be satisfactory for this purpose. Finally, the artefact-free tissue mask was combined with the grey and white matter tissue masks using logical conjunction.

2.2.5. Volumetric strain calculation

Volumetric strain maps were created as follows. First, raw phase images were extracted from the registered complex images. Second, the raw phase images were converted to displacement maps by multiplying the phase image by twice the Denc value (since the analysis was performed separately for each gradient polarity, and the Denc parameter reflects the maximum displacement which does not induce a phase wrap in the subtracted phase images, see Table 1). Third, 1D strains were computed as the gradient of the RL, AP, and FH displacement maps in the RL, AP and FH direction, respectively. Wraps in the resulting 1D strain maps (i.e. phase wraps in the displacement maps that are propagated to the 1D strain map due to the derivative operation) were spatially unwrapped under the assumption of small strains (difference in displacement between neighbouring voxels being smaller than the tag spacing). Finally, volumetric strain maps were obtained as the sum of the three 1D strains (which represents the divergence of the displacement vector field) within the 'cleaned' grey and white matter tissue masks separately. Absolute volumetric strain values greater that 1% for over half the cardiac cycle were attributed to contributions from partial-volumed CSF, remnant artefacts or large blood vessels in the tissue masks and were thus removed.

Grey and white matter volumetric strain curves were created by calculating the mean value within the volumetric strain map at each acquired cardiac phase. The volumetric strain curves obtained from the separate analysis of both gradient polarities were combined by first negating the strain curve derived from the negative gradient polarity followed by point-wise averaging. A mean, whole brain volumetric strain curve was subsequently constructed by summing the grey and white matter strain curves, weighted by the ratio of their respective tissue volumes to the whole brain tissue volume (obtained from SPM12).

2.2.6. Measurement reference adjustment

The measurement reference was adjusted to reflect tissue expansion similar to that obtained from other measurements triggered using a vectorcardiographic signal (Adams et al., 2019). This was necessary because DENSE is a measure of relative displacement accruing from the time of encoding (Aletras et al., 1999), and the signal from the POx utilised in this study is delayed relative to the vectorcardiogram (VCG). The minima of the whole brain volumetric strain curves obtained in this study were therefore set to zero and the curves were shifted to start at this beginning of the physiological cardiac cycle (close to the R-wave). Grey and white matter strain curves were also shifted temporally by the same amount.

2.2.7. CSF stroke volume analysis

The oscillating volumetric flow of CSF at the C2-C3 level was analysed as follows. A region of interest (ROI) was created using the magnitude and phase image for guidance. Phase wraps in the velocity map within the ROI were rare and were corrected through temporal unwrapping, if

present. The temporal average of the velocity map was set to zero. CSF volumetric flow was then computed as the product of the average velocity within the ROI and its area. The time integral of volumetric flow curve was calculated to obtain the CSF volume changes over the cardiac cycle. Each subject's CSF volume change curve was shifted by the same temporal offset as their respective whole brain volumetric strain curve. CSF stroke volume was defined as the peak-to-peak value of the CSF volume change curve.

2.2.8. Exploring intracranial volume dynamics

2.2.8.1. Volume change of intracranial tissue including grey and white matter differences. To investigate the intracranial tissue volume dynamics, the whole brain, grey and white matter volumetric strain curves were converted to volume changes using their respective total volume (derived from SPM). To explore physiological differences between grey and white matter tissue, the ratio of the peak grey and white matter volumetric strain curves was calculated. The time-to-peak of the volumetric strain curves was also determined.

2.2.8.2. Volume change of large intracranial vessels. A constant intracranial volume, as per the Monro-Kellie doctrine, was assumed for every phase of the cardiac cycle. The volume change of the large, intracranial vessels (summed volumes of the arterial and venous extracerebral vasculature) could then be derived from the brain and CSF volumes as defined in Eqn (2),

$$\Delta AV(t) + \Delta VV(t) = \Delta CSFV(t) - \Delta BV(t) + \Delta BSV(t) + \Delta ICV(t) \quad 1 \le t \le n \qquad \text{Eqn 2}$$

where ΔAV + ΔVV is the net volume change of the extracerebral (but intracranial) arterial and venous blood vessels. ΔCSFV and ΔBV are the CSF and brain tissue components within the cranium respectively, all at one of *n* possible frames. ΔBSV is the volume change of the brain stem displaced into the spinal canal, which was found to be negligible compared to the other components (data not shown), and thus ignored. ΔICV represents the cardiac-induced volume change of the cranial vault, which is zero (Monro-Kellie).

2.2.9. Statistics

Agreement of peak-to-peak whole brain, grey and white matter volumetric strain values from both scan sessions was assessed using Bland-Altman plots. Student's t-test was used to assess differences in the peak and time-to-peak volumetric strain values of the grey and white matter tissue. A linear regression was used to assess the relationship between cardiac-induced CSF and whole brain volume changes.

3. Results

DENSE and CSF flow measurements and analyses for all subjects were successfully completed. Fig. 1 shows example images of displacement and strain maps obtained from one subject. The observed laterally directed motion of the brain tissue arises from the use of the POx for cardiac gating and reflects tissue relaxation following the peak systolic pulse. As with previous studies (Adams et al., 2019; Pahlavian et al., 2018; Soellinger et al., 2009), larger displacements were found in the FH direction in comparison with the RL and AP directions, and typically occurred below the cerebellar tentorium. Despite the relative smoothness of the displacement maps, the strain maps were noticeably noisier in appearance.

The mean volumetric strain curves covering the entire cardiac cycle for whole brain, grey matter and white matter tissue are shown in Fig. 2. The general shape of the volumetric strain curves was similar for all measurements and subjects. The mean peak volumetric strain values obtained from the first scan session were (mean ± std): $(6.4 \pm 1.7)\times10^{-4}$ (whole brain), $(9.5 \pm 2.5)\times10^{-4}$ (grey matter), and $(4.4 \pm 1.7)\times10^{-4}$ (white matter), corresponding to peak volume changes of 0.82 ± 0.24 ml, 0.68 ± 0.20 ml and 0.24 ± 0.09 ml, respectively. The mean volumetric

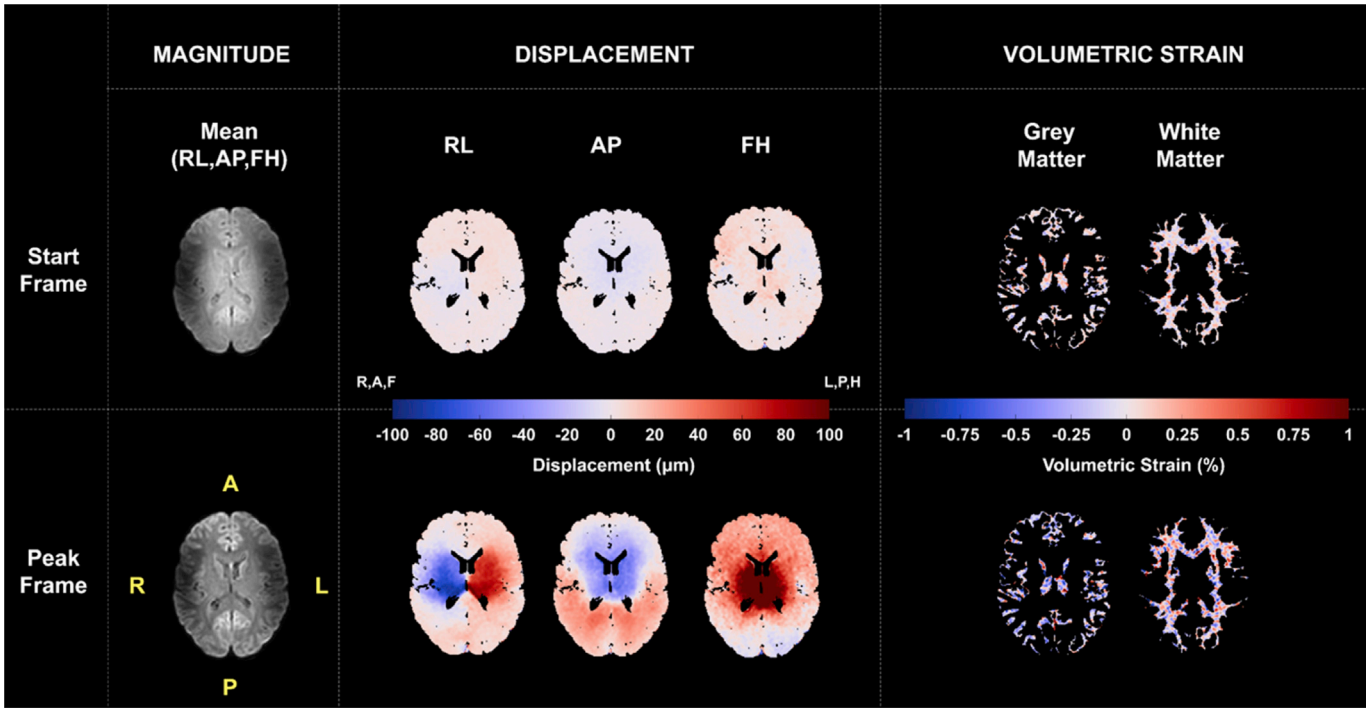

Fig. 1. Example magnitude and displacement images at the start and peak frames obtained from the retrospective DENSE acquisition triggered using a pulse oximeter. Grey and white matter volumetric strain maps are also shown. Images show displacement away from the mid-line due to the use of a pulse oximeter signal for cardiac synchronisation rather than the VCG R-wave, which yields a different reference point in the cardiac cycle for which the displacement is zero. This also results in the apparent compression observable in the strain maps.

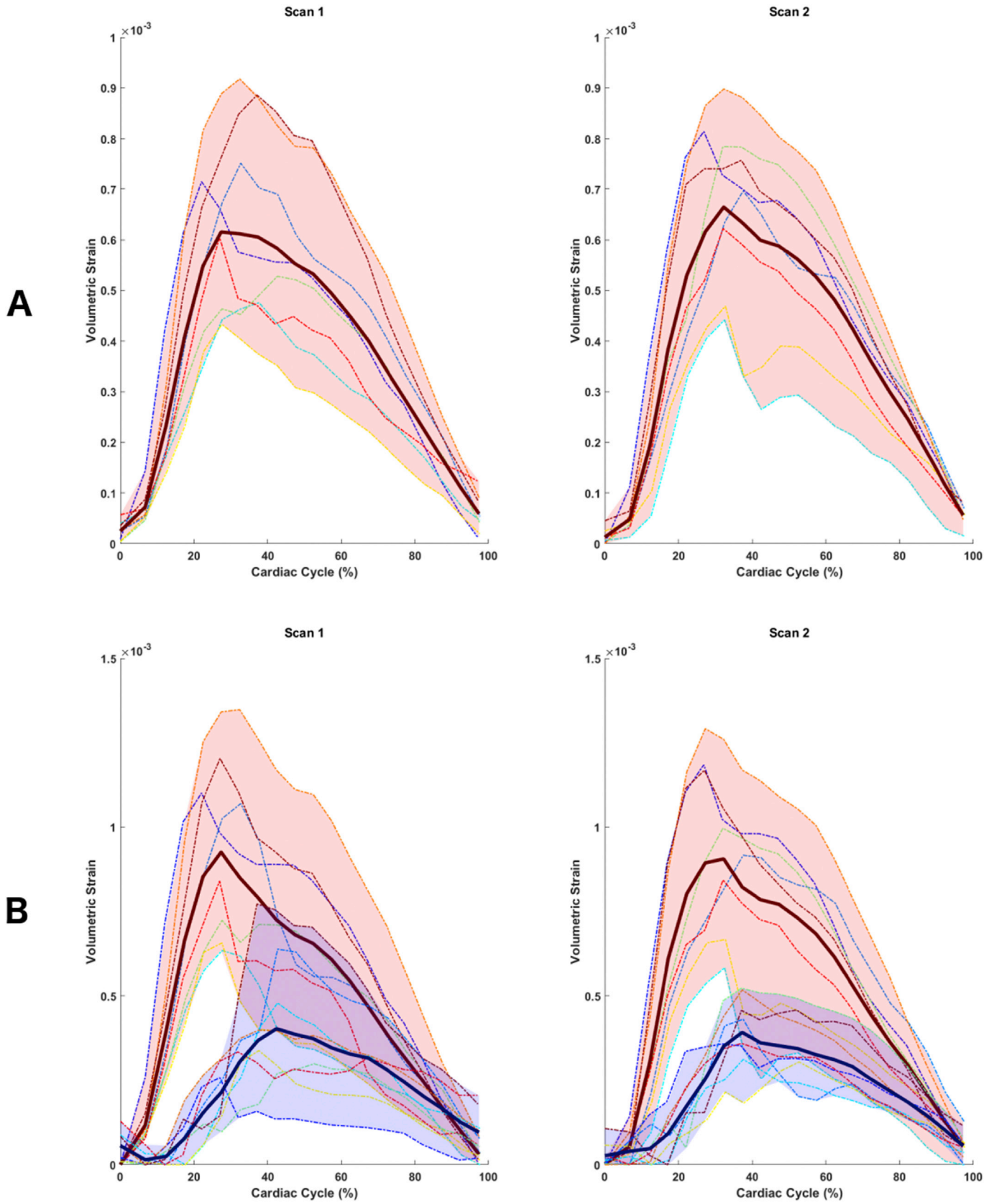

Fig. 2. Whole brain (A), and grey and white matter (B) volumetric strain curves for all subjects for the first and second scan sessions, shifted to reflect brain tissue volume changes relative to the R-wave as a reference point. The strain curves show characteristic swelling of brain during systole and relaxation during diastole. In addition to differences in their peak volumetric strain values, a delay in onset of the peak volumetric strain can be seen between grey and white matter tissue (red and blue shaded regions in B, respectively). The bold line indicates the mean over all subjects. The shaded regions around the strain curves reflect subject variability, where each subject is represented by a unique, consistent colour to aid subject comparison between scan sessions.

strain values from the first scan session were calculated using ROIs containing (32.6 ± 8.0)% and (46.4 ± 13.5)% of the available tissue for grey and white matter, respectively. For the second scan session, the mean peak volumetric strain values were: (6.7 ± 1.6)x10^{-4} (whole brain), (9.6 ± 2.4)x10^{-4} (grey matter) and (4.1 ± 0.8)x10^{-4} (white matter), corresponding to peak volume changes of 0.86 ± 0.22 ml, 0.69 ± 0.19 ml and 0.23 ± 0.05 ml, respectively. The mean volumetric strain values from the second scan session were calculated using ROIs containing (36.4 ± 3.7)% and (52.9 ± 6.7)% of the available tissue for grey and white matter, respectively.

Fig. 3 shows Bland-Altman plots of the mean peak volumetric strain values for whole brain, grey and white matter tissue from both scan sessions. The mean peak grey matter volumetric strain values were observed to have a higher inter-subject variability than those of white matter.

A good agreement was found between the changes in the CSF and brain volumes over the cardiac cycle for all subjects (see Table 2 and Fig. 4). Linear regression of CSF vs whole brain tissue volume changes yielded a mean slope of 0.88 ± 0.23 with an R^2 value of 0.89 ± 0.07. The mean peak CSF stroke volume was 0.74 ± 0.33 ml. The derived volume changes of the large intracranial vessels were relatively limited, with a mean stroke volume of 0.33 ± 0.10 ml. The volume changes of the CSF, brain and large intracranial vessels over the entire cardiac cycle are shown in Fig. 5.

The mean peak volumetric strain of grey matter was significantly higher than that of white matter, with a p-value < 0.001 in both scan sessions. The peak grey to white matter volumetric strain ratio was 2.4 ± 0.9 (first scan session) and 2.3 ± 0.4 (second scan session). After correcting for the delay between the pulse oximeter and VCG R-wave, the mean peak whole brain volumetric strain occurred at (mean ± std) (32.4 ± 6.3)% and (32.9 ± 3.1)% of the cardiac cycle for the first and second scan sessions, respectively. For both scan sessions, the time-to-peak for grey and white matter was found to be significantly different. For the first scan session, mean grey and white matter volumetric strain peaked at (28.0 ± 3.2)% and (38.6 ± 7.2)% of the cardiac cycle, respectively (p-value < 0.004). In the second scan session, the peak value for grey and white matter occurred at (31.0 ± 3.5)% and (40.4 ± 7.1)% of the cardiac cycle, respectively (p-value < 0.02).

Table 2
Results of the linear regression analysis of the cardiac-induced CSF and brain tissue volume changes for each subject in this study.

Subjects	Slope	Intercept	R^2	RMSE
1	1.09	0.07	0.91	0.10
2	1.15	0.04	0.96	0.07
3	0.74	0.05	0.95	0.03
4	0.69	−0.01	0.89	0.05
5	0.60	0.00	0.88	0.04
6	0.70	0.05	0.84	0.12
7	0.86	0.04	0.75	0.08
8	1.19	0.07	0.97	0.08
(Mean ± std)	**0.88 ± 0.23**	**0.04 ± 0.03**	**0.89 ± 0.07**	**0.07 ± 0.03**

4. Discussion

We validated a faster DENSE implementation as a method for quantifying cardiac-induced brain tissue pulsations. Shorter scan durations were achieved through the use of a retrospectively-gated implementation of DENSE. The peak brain tissue volumetric strain value was found to be consistent between repeated measurements for whole brain and grey matter, and fairly consistent for white matter. Additionally, the brain tissue volume changes agreed well with independent measures of CSF volume change in the same subjects. The DENSE and CSF measurements were used to further explore intracranial volume dynamics. Relative to white matter, grey matter showed a considerably higher peak volume change that occurred considerably earlier in the cardiac cycle. Under the assumption of a fixed intracranial volume and the incompressible tissue constituents of the cranial vault, we inferred a relatively small net contribution of the large intracranial extracerebral vessels (having a diameter in the order of 1 mm and more) to the CSF volume expelled towards the spinal canal during the cardiac cycle.

A retrospectively-gated implementation of DENSE was used in this study to expand on the early work on cardiac-driven pulsatile brain motion established by previous authors such as (Feinberg and Mark, 1987), (Greitz et al., 1992), and others more recently (Adams et al., 2019; Pahlavian et al., 2018; Soellinger et al., 2009). In comparison with our previous work utilizing DENSE to acquire cardiac-induced brain tissue motion (Adams et al., 2019), the retrospectively-gated implementation of DENSE reduced the scan duration by half whilst still achieving a similar SNR (Adams et al., 2018). The reduced scan time not only improves its candidacy for use in clinical research, but also reduces potential subject-based motion artefacts. Although the retrospectively-gated algorithm is compatible with the use of a VCG signal for cardiac synchronisation, utilisation of the POx instead simplifies measurement setup whilst providing a stable signal, free from magnetohydrodynamic artefacts. A minor consequence of using the POx in this manner is an implied compression of brain tissue due to the peak-systolic cardiac phase used as a reference point for triggering the DENSE measurements. As shown in this study, this issue can be easily corrected in post-processing.

The Bland-Altman analysis revealed good agreement of peak brain

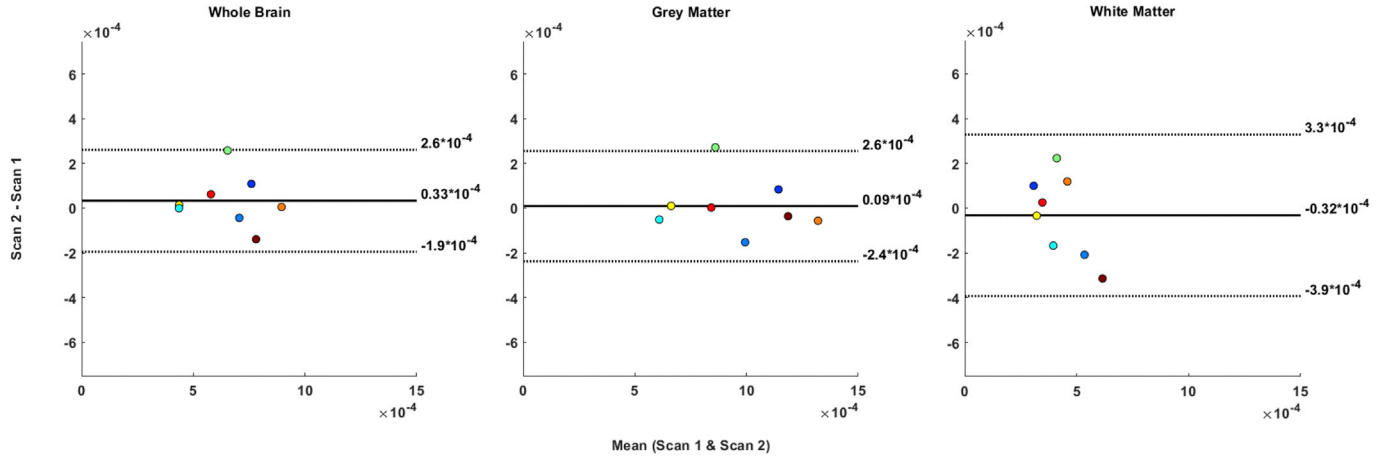

Fig. 3. Bland-Altman plot showing the repeatability of whole brain, grey and white matter peak volumetric strains. The dotted lines indicate the limits of agreement (1.96 x standard deviation), whilst the bold line indicates the mean difference. Each colour represents a specific subject.

tissue volumetric strain between measurements. We observed lower SNR at the centre of the brain due to the lower sensitivity of the receive coil array. This lower SNR, in addition to the generally lower mean peak volumetric strain values may explain the limited repeatability observed in this study for white matter. Nonetheless, the high repeatability of the peak whole brain volumetric strain, in conjunction with the high correlation to CSF volume changes, suggests that the variability in peak volumetric strain observed amongst subjects reflects physiological variation rather than measurement error. Due to the relatively long acquisition, respiration effects are averaged out, thus its impact on the variation observed in this study was limited. It should be noted that from our previous work (Adams et al., 2019), it was estimated that increasing the DENSE SNR by a factor of ~10 allows for a voxel-wise analysis of the peak volumetric strain. In terms of SNR, this is equivalent to averaging ~100 voxels. Therefore, in this study spatial smoothing of the data was unnecessary since results were obtained from averaging over 10k voxels.

The approximately linear relationship (as obtained from the regression analysis) between CSF and brain tissue volume changes is consistent with current concepts of intracranial volume change. In order to compensate for the increased blood volume which enters the cranium from the heart during each cardiac cycle, a similar volume of CSF is flushed out into the spinal canal, thereby assisting with the maintenance of a stable intracranial pressure (Alperin et al., 1996; Balédent et al., 2001; Capel et al., 2018; Enzmann and Pelc, 1993). Thus, if only the average brain volume change is of interest, one might use CSF stroke volume measurements at the level of the spinal canal, which are shown to be readily available at clinical field strengths (Balédent et al., 2001). The internal validation of our method using CSF volume changes increases confidence in the volume change measurements obtained using DENSE, despite the inherent sensitivity of the volumetric strain calculation to noise.

Exploration of the volume changes in the large intracranial vessels was achievable using the results obtained from the internal validation of our method. Fundamental to the exploration of these volume changes is the notion of intracranial volume change (ICVC). Several investigators have previously calculated ICVCs by summing transcranial blood and CSF flows into and out of the cranium over the cardiac cycle. Based on this approach, average maximum ICVCs of 0.6 ± 0.1 ml (Balédent et al., 2006), 0.48 ± 0.15 ml (Alperin et al., 2005) and 0.43 ± 0.12 ml (Tsai et al., 2018) have been reported. Our results are complementary to these measurements as we quantified the contribution of the swelling of the vasculature embedded in the brain tissue to the CSF expelled in the spinal canal. Considering these vessels to belong by definition to the microvasculature, we estimated the swelling of the extracerebral vasculature (or intracranial 'macrovasculature') by subtracting the brain tissue volume from the CSF volume. This estimation is based on the assumption that the intracranial volume is truly rigid and does not show a volume change over the cardiac cycle. We believe that this is a valid assumption since the skull is three orders of magnitude stiffer (Peterson and Dechow, 2003) than the brain tissue (Jin et al., 2013). Even in the soft brain tissue, only a volume change of about 1 ml is observed. However, if the estimated ICVCs in the literature are realistic (or reflect tissue and/or fluid flows through other foramina), such ICVCs have to be added to our estimated macrovascular volume pulsations. This still would yield stroke volumes of the large intracranial vessels of similar size as the stroke volume of the microvasculature, underscoring that the contribution of the microvasculature cannot be ignored. On the other hand, if the ICVC truly is negligible, our findings of limited volume change in the large intracranial (but extracerebral) blood vessels implies compression of the cortical veins and cavernous sinus. In either case, direct measurements of the blood volume changes in the extracerebral macrovascular are challenging due to the complex venous drainage system (Schaller, 2004).

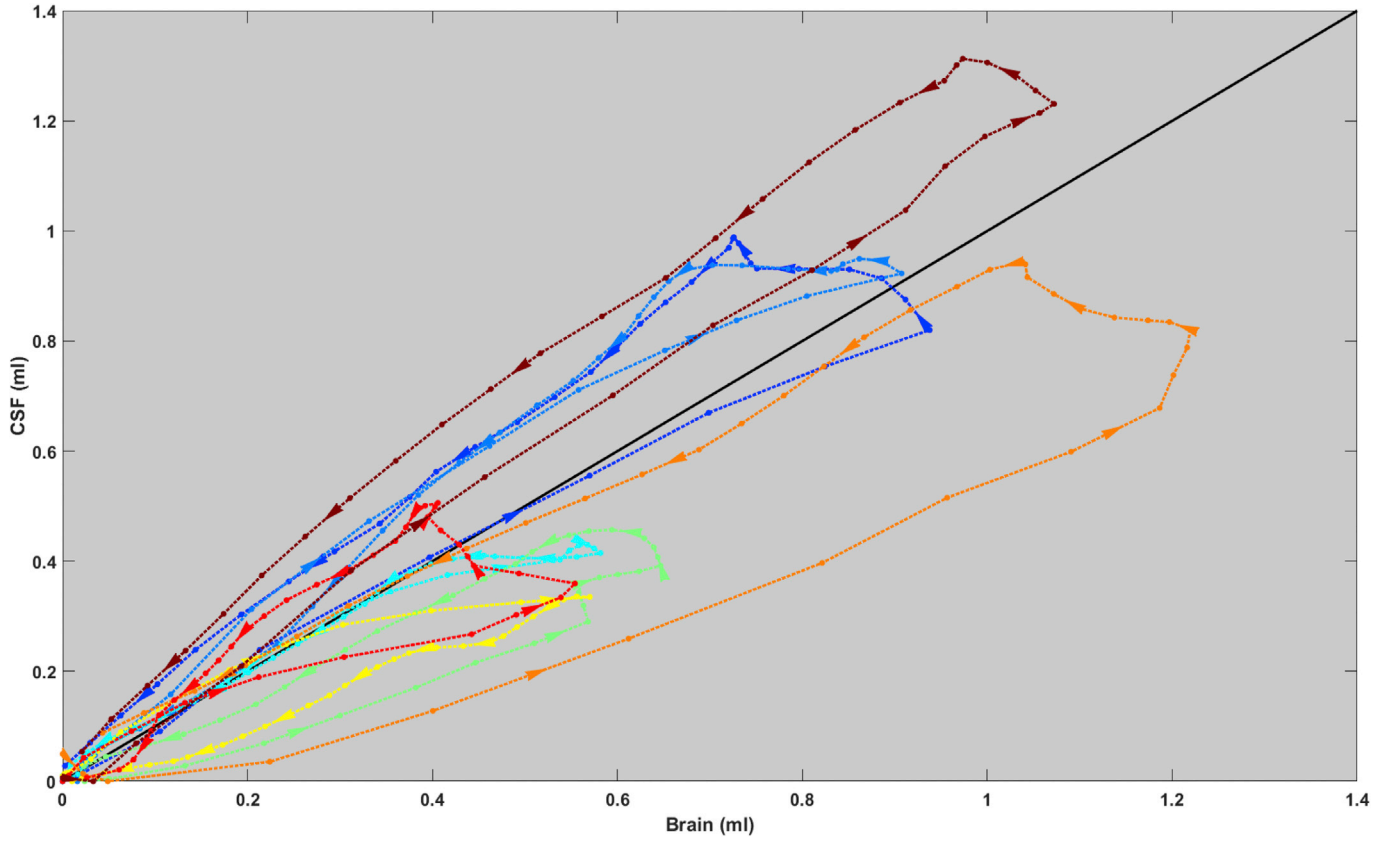

Fig. 4. CSF vs brain tissue volume changes over the measured cardiac cycle. The black solid line represents y = x. Each coloured line represents a specific subject. Larger dots on the lines signify measurement points. A hysteresis effect is noticeable, with the direction indicated by the arrow heads.

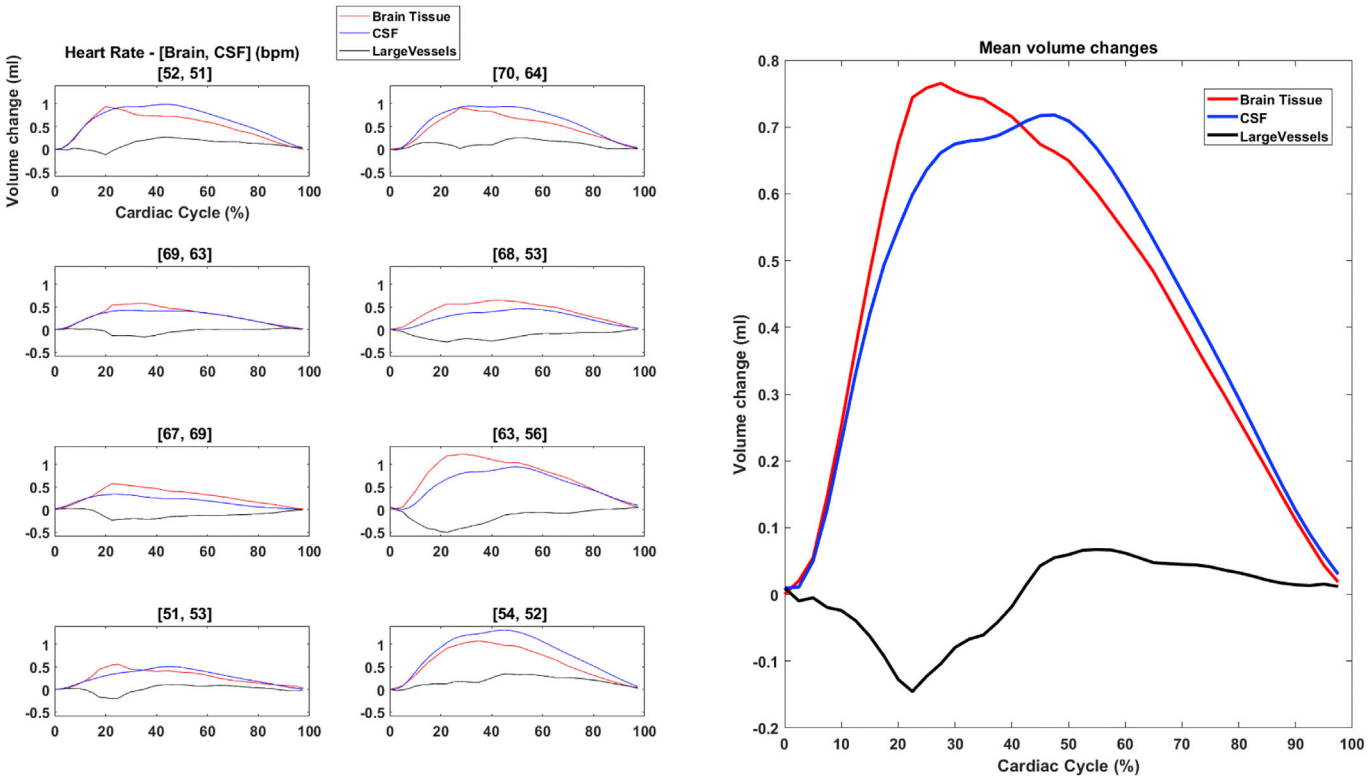

Fig. 5. Brain and CSF volume changes over the cardiac cycle for all subjects. Positive values of the CSF volume change curve indicate volume displaced into the spinal canal. The estimated contribution of the large intracranial vessels (including both arteries and veins) is also shown. The mean heart rate during measurements of the brain and CSF volume changes is indicated between brackets above each figure.

Therefore, the method of indirect estimation as performed in our study may provide a means to gain further insights into the intracranial volume dynamics. We observed a net negative volume of the extracerebral macrovascular compartment during systole, which may reflect an initial venous compression (DE Simone et al., 2017; Enzmann and Pelc, 1993; Greitz, 2006) due to the rapid increase in intracranial pressure (Alperin et al., 2006), before the CSF can be displaced. As such, due to the tightly coupled pressure-volume relationships between the incompressible constituents of the cranial cavity, reduced or abnormal CSF expulsion, such as that which occurs in the elderly (Stoquart-ElSankari et al., 2007) or in disorders such as Chiari I malformation (Haughton et al., 2003), may be associated with altered microvascular pulsations within the brain tissue. Altered microvascular pulsations may also occur as a result of intracranial hypertension (Saindane et al., 2018), hydrocephalus and age-related 'pulse wave encephalopathy' (Cecile Henry-Feugeas and Koskas, 2012).

The measured differences in the mean volumetric strain value of grey and white matter tissue reflects the physiological differences between these two tissue types. Since white matter is stiffer than grey matter (Jin et al., 2013), the lower volumetric strain (or, equivalently, volume change) for the former obtained in this study may not only reflect differences in the blood volume occupying both tissue types, but also differences in tissue viscoelasticity. The vascular organization within the brain parenchyma results in grey matter being perfused before white matter, and intuitively provides an explanation for the delay observed between peak grey and white matter volumetric strain. However, given the speed of the arterial pulse wave, and the mean distance between the two tissue types, it is unlikely that this delay can be measured with the temporal resolution used in this study. Rather, a more likely explanation for the observed delay in peak swelling between grey and white matter can be surmised from the BOLD-CVR studies performed by (Bhogal et al., 2015), where it was suggested that grey matter is preferentially filled with blood due to its denser vascularization. Therefore, grey matter may buffer cardiac-induced blood volume changes before these are redirected to the white matter. It is unclear how the surrounding tissue stiffness properties affect the propagation of the arterial pulse wave throughout the microvasculature. One approach may be to lump tissue and vessel wall stiffness as a single parameter in biomechanical modelling (Ambarki et al., 2007), which is outside the scope of this paper.

Our results are similar to those reported in the literature. The peak volumetric strain values obtained in this study are in agreement with previous measurements of tissue volumetric strain using prospectively-triggered DENSE (Adams et al., 2019) and PCMRI (Hirsch et al., 2013). Furthermore, the peak grey to white matter volume change ratio of approximately 2.4 found in this study is similar to that obtained in other MR based methods of assessing brain tissue blood volume variations over the cardiac cycle. (Viessmann et al., 2017) assessed the signal fluctuations derived from double-echo EPI scans and found an approximate factor of 2 in the T2* fluctuations of grey and white matter, with the former being larger. They associated these T2* fluctuations with blood volume changes between these two tissue types. Interestingly, they also observed phase delays between different grey matter regions but do not report such a relation between grey and white matter. (Rivera-Rivera et al., 2019) also investigated brain tissue blood volume differences using T2* signal fluctuations, enhanced through the use of ferumoxytol as a contrast agent and instead obtained through a spiral acquisition. As in this study, they also obtained a significant difference between grey and white matter blood volume pulsations over the cardiac cycle, however they found a slightly lower ratio of approximately 1.6. The ratio they obtained may have been limited by the model used to estimate brain volume changes. They also do not report any differences in the time to peak of grey and white matter microvascular blood volumes, which may be due to the reconstructed temporal resolution and retrospective binning used in that study. The group mean CSF stroke volume

measurements achieved in our study are also similar to those obtained by other investigators using PCMRI to measure volumetric CSF flow at the C2-C3 cervical level: 0.58 ± 0.12 ml (Balédent, 2014), 0.71 ± 0.32 ml (Wåhlin et al., 2014), 0.77 ± 0.23 ml (Wåhlin et al., 2012).

Cerebral small vessel disease is an age-linked, neurological disorder characterized by damage to the microvasculature and the surrounding tissue bed (Shi and Wardlaw, 2016). As such, brain tissue volumetric strain measurements, which uniquely contain joint information on both vascular and tissue function, may prove to be a useful tool for investigating early pathological changes induced by this disease, conceivably even before the vascular/neuronal damage is visible on typical CT/MR images. Moreover, cardiac pulsation is claimed to be involved in the brain's clearance system (Iliff et al., 2013). Although it is unlikely that cardiac pulsation drives a net fluid flow in the tissue, it is well conceivable that the observed tissue deformations contribute to mixing of fluids and, thus, to more effective waste transport (Asgari et al., 2016; Bedussi et al., 2018). In this study we observed consistency between repeated measurements of brain tissue volumetric strain, and also internal consistency of brain tissue and CSF intracranial volume exchange in accordance to the Monro-Kellie doctrine. These consistencies together strengthen the potential of this method as a biomarker of the microvascular function for investigating the ageing brain under healthy and diseased conditions. Our measurements also revealed an inter-subject variation, which is likely related to physiological differences, including inter-subject variation in intracranial pressure (Saindane et al., 2018). Future work is warranted to explore these differences to determine whether a particular physiology may be linked to age, sex and/or risk factors for disorders such as stroke or cerebral small vessel disease. Additionally, given the existing inter-subject variation in controls, future studies comparing matched controls with patients or elderly are needed to investigate the power of this technique for detecting disease or changes with age (where a reduction in tissue strain is expected given CSF stroke volume reduction with age (Stoquart-ElSankari et al., 2007)).

Several biomechanical phenomena underlie the volumetric strain values reported in this study: the change in blood volume of the microvasculature within the parenchyma (Sweetman and Linninger, 2011), the net pulsatile pressure acting on the parenchyma (Mousavi et al., 2014) and the parenchyma's viscoelastic properties (Hirsch et al., 2013). As previously discussed, our volumetric strain measurements may provide early insights into diseases which alter those underlying phenomena. Moreover, in some cases, minor differences in cardiac-induced pulsatile pressure may be assumed throughout the brain parenchyma (Eide, 2008). Under that assumption, the parenchymal viscoelastic properties can be approximated using MR elastography reconstructions derived from displacement measurements such as those acquired in this study (Weaver et al., 2012; Zorgani et al., 2015). This would in principle allow the disentanglement of the tissue volume change from its viscoelastic properties, allowing separate quantification of changes to these specific biomechanical phenomena due to age or disease. Future work is also warranted to explore how cardiac-induced brain tissue volumetric strain measurements depend on the actual physiology during the measurements such as heart rate and respiration rate, which may vary based on the level of anxiety of the patient in the scanner.

Due to the sensitivity required to accurately measure brain tissue displacement, which would introduce multiple phase-wraps of CSF motion at the C2-C3 level, simultaneous measurements of brain tissue and CSF motion from the DENSE images were not possible. In some subjects we noted a discrepancy in the average heart-rate between DENSE and CSF measurements (see Fig. 5). CSF and arterial flow waveforms are known to be a function of heart rate (Daouk et al., 2017; Strik et al., 2002). The heart rate discrepancy may thus restrict interpretations of the brain tissue and CSF intracranial volume imbalance.

As with other measurements of brain tissue using DENSE (Adams et al., 2019; Soellinger et al., 2009), some images contained artefacts which may be related to the SENSE acceleration, intra-voxel dephasing, and subject motion including respiration. Although these artefact regions were excluded from the analysis, their removal may have hampered measurement repeatability by the exclusion of volumetric strain data from key brain regions. The removal of these artefacts, and an increase in measurement SNR would further allow brain region volumetric strain analyses using smaller ROIs, and is the focus of future work. A further limitation of this study is the use of registration software to correct for EPI distortions, which could be improved through the use of an acquired B0-field map.

5. Conclusion

Cardiac-induced brain tissue pulsatility has consistent inter-subject peak values in repeated measurements of healthy subjects. Furthermore, it is strongly correlated to CSF volume changes measured at the C2-C3 level. The successful internal validation of measured brain volume changes to CSF displaced into the spinal canal suggests that due to venous compression, the extracerebral macrovasculature offers a relatively minor contribution to CSF intracranial dynamics over the cardiac cycle. The consistency between repeated brain tissue volumetric strain measurements, and internal validation to CSF measurements strengthens the potential of brain tissue volumetric strain as a tool for investigating the ageing brain in normal or diseased states.

Funding

This work was supported by the European Research Council, ERC grant agreement n°337333. The funding source had no involvement in the study design, nor in the collection, analysis and interpretation of data, nor in the writing of the report, nor in the decision to submit the article for publication.

Declaration of competing interest

The authors have no conflict of interests to disclose.

Acknowledgements

The authors thank Hugo Kuijf and Martijn Froeling for helpful discussions. The authors are also grateful to Jacob-Jan Sloots for assistance with the implementation of retrospectively-gated DENSE and the MR acquisitions.

Appendix A. Supplementary data

Supplementary data to this article can be found online at https://doi.org/10.1016/j.neuroimage.2019.116466.

References

Adams, A.L., Kuijf, H.J., Viergever, M.A., Luijten, P.R., Zwanenburg, J.J.M., 2019. Quantifying cardiac-induced brain tissue expansion using DENSE. NMR Biomed. 32, 1–13. https://doi.org/10.1002/nbm.4050.

Adams, A.L., Sloots, J.-J., Luijten, P.R., Zwanenburg, J.J.M., 2018. SNR analysis of retrospectively gated DENSE at 7T for the measurement of brain tissue pulsatility. In: Proceedings of the Joint Annual Meeting ISMRM-ESMRMB. Paris, France.

Aletras, A.H., Ding, S., Balaban, R.S., Wen, H., 1999. DENSE: displacement encoding with stimulated Echoes in cardiac functional MRI. J. Magn. Reson. 137, 247–252. https://doi.org/10.1006/jmre.1998.1676.

Alperin, N., Lee, S.H., Sivaramakrishnan, A., Hushek, S.G., 2005. Quantifying the effect of posture on intracranial physiology in humans by MRI flow studies. J. Magn. Reson. Imaging 22, 591–596. https://doi.org/10.1002/jmri.20427.

Alperin, N., Mazda, M., Lichtor, T., Lee, S.H., 2006. From cerebrospinal fluid pulsation to noninvasive intracranial compliance and pressure measured by MRI flow studies. Curr. Med. Imag. Rev. 2, 117–129. https://doi.org/10.2174/157340506775541622.

Alperin, N., Vikingstad, E.M., Gomez-Anson, B., Levin, D.N., 1996. Hemodynamically independent analysis of cerebrospinal fluid and brain motion observed with dynamic phase contrast MRI. Magn. Reson. Med. 35, 741–754. https://doi.org/10.1002/mrm.1910350516.

Ambarki, K., Baledent, O., Kongolo, G., Bouzerar, R., Fall, S., Meyer, M.E., 2007. A new lumped-parameter model of cerebrospinal hydrodynamics during the cardiac cycle in

healthy volunteers. IEEE Trans. Biomed. Eng. 54, 483–491. https://doi.org/10.1109/TBME.2006.890492.
Asgari, M., De Zélicourt, D., Kurtcuoglu, V., 2016. Glymphatic solute transport does not require bulk flow. Sci. Rep. 6, 1–11. https://doi.org/10.1038/srep38635.
Balédent, O., 2014. Imaging of the cerebrospinal fluid circulation. In: Rigamonti, D. (Ed.), Adult Hydrocephalus. Cambridge University Press, Cambridge, pp. 121–138. https://doi.org/10.1017/CBO9781139382816.013.
Balédent, O., Fin, L., Khuoy, L., Ambarki, K., Gauvin, A.-C., Gondry-Jouet, C., Meyer, M.-E., 2006. Brain hydrodynamics study by phase-contrast magnetic resonance imaging and transcranial color doppler. J. Magn. Reson. Imaging 24, 995–1004. https://doi.org/10.1002/jmri.20722.
Balédent, O., Henry-Feugeas, M.C., Idy-Peretti, I., 2001. Cerebrospinal fluid dynamics and relation with blood flow: a magnetic resonance study with semiautomated cerebrospinal fluid segmentation. Investig. Radiol. 36, 368–377. https://doi.org/10.1097/00004424-200107000-00003.
Bedussi, B., Almasian, M., de Vos, J., VanBavel, E., Bakker, E.N.T.P., 2018. Paravascular spaces at the brain surface: low resistance pathways for cerebrospinal fluid flow. J. Cereb. Blood Flow Metab. 38, 719–726. https://doi.org/10.1177/0271678X17737984.
Bhogal, A.A., Philippens, M.E.P., Siero, J.C.W., Fisher, J.A., Petersen, E.T., Luijten, P.R., Hoogduin, H., 2015. Examining the regional and cerebral depth-dependent BOLD cerebrovascular reactivity response at 7T. Neuroimage 114, 239–248. https://doi.org/10.1016/j.neuroimage.2015.04.014.
Capel, C., Baroncini, M., Gondry-Jouet, C., Bouzerar, R., Czosnyka, M., Czosnyka, Z., Balédent, O., 2018. Cerebrospinal fluid and cerebral blood flows in idiopathic intracranial hypertension. In: Acta Neurochirurgica, Supplementum, pp. 237–241. https://doi.org/10.1007/978-3-319-65798-1_48.
Henry-Feugeas, M.Cecile, Koskas, P., 2012. Cerebral Vascular Aging: Extending the Concept of Pulse Wave Encephalopathy Through Capillaries to the Cerebral Veins. Current Aging Science 5 (2). https://doi.org/10.2174/1874609811205020157.
Daouk, J., Bouzerar, R., Baledent, O., 2017. Heart rate and respiration influence on macroscopic blood and CSF flows. Acta Radiol. 58, 977–982. https://doi.org/10.1177/0284185116676655.
DE Simone, R., Ranieri, A., Bonavita, V., 2017. Starling resistors, autoregulation of cerebral perfusion and the pathogenesis of idiopathic intracranial hypertension. Panminerva Med. 59, 76–89. https://doi.org/10.23736/S0031-0808.16.03248-1.
Eide, P.K., 2008. Comparison of simultaneous continuous intracranial pressure (ICP) signals from ICP sensors placed within the brain parenchyma and the epidural space. Med. Eng. Phys. 30, 34–40. https://doi.org/10.1016/j.medengphy.2007.01.005.
Enzmann, D.R., Pelc, N.J., 1993. Cerebrospinal fluid flow measured by phase-contrast cine MR. AJNR. Am. J. Neuroradiol. 14, 1301–1307.
Feinberg, D.A., Mark, A.S., 1987. Human brain motion and cerebrospinal fluid circulation demonstrated with MR velocity imaging. Radiology 163, 793–799. https://doi.org/10.1148/radiology.163.3.3575734.
Greitz, D., 2006. Radiological assessment of hydrocephalus: new theories and implications for therapy. Neuroradiol. J. 19, 475–495. https://doi.org/10.1177/197140090601900407.
Greitz, D., Wirestam, R., Franck, A., Nordell, B., Thomsen, C., Stahlberg, F., 1992. Pulsatile brain movement and associated hydrodynamics studied by magnetic resonance phase imaging. Neuroradiology 34, 370–380. https://doi.org/10.1007/BF00596493.
Haughton, V.M., Korosec, F.R., Medow, J.E., Dolar, M.T., Iskandar, B.J., 2003. Peak systolic and diastolic CSF velocity in the foramen magnum in adult patients with Chiari I malformations and in normal control participants. Am. J. Neuroradiol. 24, 169–176.
Hirsch, S., Klatt, D., Freimann, F., Scheel, M., Braun, J., Sack, I., 2013. In vivo measurement of volumetric strain in the human brain induced by arterial pulsation and harmonic waves. Magn. Reson. Med. 70, 671–683. https://doi.org/10.1002/mrm.24499.
Iliff, J.J., Wang, M., Zeppenfeld, D.M., Venkataraman, A., Plog, B.A., Liao, Y., Deane, R., Nedergaard, M., 2013. Cerebral arterial pulsation drives paravascular CSF-interstitial fluid exchange in the murine brain. J. Neurosci. 33, 18190–18199. https://doi.org/10.1523/JNEUROSCI.1592-13.2013.
Jin, X., Zhu, F., Mao, H., Shen, M., Yang, K.H., 2013. A comprehensive experimental study on material properties of human brain tissue. J. Biomech. 46, 2795–2801. https://doi.org/10.1016/j.jbiomech.2013.09.001.
Klein, S., Staring, M., Murphy, K., Viergever, M.A., Pluim, J., 2010. Elastix: a Toolbox for intensity-based medical image registration. IEEE Trans. Med. Imaging 29, 196–205. https://doi.org/10.1109/TMI.2009.2035616.
Mousavi, S.R., Fehlner, A., Streitberger, K.J., Braun, J., Samani, A., Sack, I., 2014. Measurement of in vivo cerebral volumetric strain induced by the Valsalva maneuver. J. Biomech. 47, 1652–1657. https://doi.org/10.1016/j.jbiomech.2014.02.038.
Pahlavian, S.H., Oshinski, J., Zhong, X., Loth, F., Amini, R., 2018. Regional quantification of brain tissue strain using displacement-encoding with stimulated Echoes magnetic resonance imaging. J. Biomech. Eng. 140, 081010 https://doi.org/10.1115/1.4040227.
Peterson, J., Dechow, P.C., 2003. Material properties of the human cranial vault and zygoma. Anat. Rec. Part A Discov. Mol. Cell. Evol. Biol. 274, 785–797. https://doi.org/10.1002/ar.a.10096.
Rivera-Rivera, L.A., Johnson, K.M., Turski, P.A., Wieben, O., Schubert, T., 2019. Measurement of microvascular cerebral blood volume changes over the cardiac cycle with ferumoxytol-enhanced T 2 * MRI. Magn. Reson. Med. 1–11. https://doi.org/10.1002/mrm.27670.
Saindane, A.M., Qiu, D., Oshinski, J.N., Newman, N.J., Biousse, V., Bruce, B.B., Holbrook, J.F., Dale, B.M., Zhong, X., 2018. Noninvasive assessment of intracranial pressure status in idiopathic intracranial hypertension using displacement encoding with stimulated Echoes (DENSE) MRI: a prospective patient study with contemporaneous CSF pressure correlation. Am. J. Neuroradiol. 39, 311–316. https://doi.org/10.3174/ajnr.A5486.
Schaller, B., 2004. Physiology of cerebral venous blood flow: from experimental data in animals to normal function in humans. Brain Res. Rev. 46, 243–260. https://doi.org/10.1016/j.brainresrev.2004.04.005.
Shi, Y., Wardlaw, J.M., 2016. Update on cerebral small vessel disease: a dynamic whole-brain disease. BMJ 1, 83–92. https://doi.org/10.1136/svn-2016-000035.
Sloots, J.-J., Adams, A.L., Luijten, P.R., Biessels, G.J., Zwanenburg, J.J.M., 2018. Unraveling cardiac and respiratory contributions to brain tissue motion using single shot 2D DENSE at 7T MRI. In: Proceedings of the Joint Annual Meeting ISMRM-ESMRMB. Paris.
Soellinger, M., Rutz, A.K., Kozerke, S., Boesiger, P., 2009. 3D cine displacement-encoded MRI of pulsatile brain motion. Magn. Reson. Med. 61, 153–162. https://doi.org/10.1002/mrm.21802.
Stoquart-ElSankari, S., Balédent, O., Gondry-Jouet, C., Makki, M., Godefroy, O., Meyer, M.-E., 2007. Aging effects on cerebral blood and cerebrospinal fluid flows. J. Cereb. Blood Flow Metab. 27, 1563–1572. https://doi.org/10.1038/sj.jcbfm.9600462.
Strik, C., Klose, U., Erb, M., Strik, H., Grodd, W., 2002. Intracranial oscillations of cerebrospinal fluid and blood flows: analysis with magnetic resonance imaging. J. Magn. Reson. Imaging 15, 251–258. https://doi.org/10.1002/jmri.10084.
Stuber, M., Spiegel, M.A., Fischer, S.E., Scheidegger, M.B., Danias, P.G., Pedersen, E.M., Boesiger, P., 1999. Single breath-hold slice-following CSPAMM myocardial tagging. Magn. Reson. Mater. Phys. Biol. Med. 9, 85–91. https://doi.org/10.1016/S1352-8661(99)00049-6.
Sweetman, B., Linninger, A.A., 2011. Cerebrospinal fluid flow dynamics in the central nervous system. Ann. Biomed. Eng. 39, 484–496. https://doi.org/10.1007/s10439-010-0141-0.
Tsai, Y.H., Chen, H.C., Tung, H., Wu, Y.Y., Chen, H.M., Pan, K.J., Cheng, D.C., Chen, J.H., Chen, C.C.C., Chai, J.W., Shen, W.C., 2018. Noninvasive assessment of intracranial elastance and pressure in spontaneous intracranial hypotension by MRI. J. Magn. Reson. Imaging 1–9. https://doi.org/10.1002/jmri.25976.
Viessmann, O., Möller, H.E., Jezzard, P., 2017. Cardiac cycle-induced EPI time series fluctuations in the brain: their temporal shifts, inflow effects and T2*fluctuations. Neuroimage 162, 93–105. https://doi.org/10.1016/j.neuroimage.2017.08.061.
Wåhlin, A., Ambarki, K., Birgander, R., Malm, J., Eklund, A., 2014. Intracranial pulsatility is associated with regional brain volume in elderly individuals. Neurobiol. Aging 35, 365–372. https://doi.org/10.1016/j.neurobiolaging.2013.08.026.
Wåhlin, A., Ambarki, K., Hauksson, J., Birgander, R., Malm, J., Eklund, A., 2012. Phase contrast MRI quantification of pulsatile volumes of brain arteries, veins, and cerebrospinal fluids compartments: repeatability and physiological interactions. J. Magn. Reson. Imaging 35, 1055–1062. https://doi.org/10.1002/jmri.23527.
Weaver, J.B., Pattison, A.J., McGarry, M.D., Perreard, I.M., Swienckowski, J.G., Eskey, C.J., Lollis, S.S., Paulsen, K.D., 2012. Brain mechanical property measurement using MRE with intrinsic activation. Phys. Med. Biol. 57, 7275–7287. https://doi.org/10.1088/0031-9155/57/22/7275.
Zorgani, A., Souchon, R., Dinh, A.-H., Chapelon, J.-Y., Ménager, J.-M., Lounis, S., Rouvière, O., Catheline, S., 2015. Brain palpation from physiological vibrations using MRI. Proc. Natl. Acad. Sci. 112, 12917–12921. https://doi.org/10.1073/pnas.1509895112.